Geotech Geol Eng (2015) 33:795–812
DOI 10.1007/s10706-015-9860-1

ORIGINAL PAPER

Seismic Active Earth Pressure on Walls Using a New Pseudo-Dynamic Approach

Ivo Bellezza

Received: 4 August 2014 / Accepted: 7 February 2015 / Published online: 17 February 2015

Abstract Seismic active soil thrust, soil pressure distribution and overturning moment are obtained in closed form using a new pseudo-dynamic approach based on standing shear and primary waves propagating on a visco-elastic backfill overlying rigid bedrock subjected to both harmonic horizontal and vertical acceleration. Seismic waves respect the zero stress boundary condition at the soil surface, backfill is modeled as a Kelvin–Voigt medium and a planar failure surface is assumed in the analysis. Effects of a wide range of parameters such as amplitude of base accelerations, soil shear resistance angle, soil wall friction angle, damping ratio are discussed. Results of the parametric study indicate that amplitude of the horizontal base acceleration and soil shear resistance angle are the factors most influencing active pressure distribution whereas the presence of the vertical acceleration always results in a quite small increase in seismic active thrust. Damping ratio is important mainly close to the fundamental frequency of shear wave where seismic active thrust is maximum. Unlike the original pseudo-dynamic approach the effect of a different frequency for S-wave and P-wave is considered in the analysis. Seismic active thrust is found to increase when the frequency of P-wave is greater than that of S-wave. The results obtained by the proposed approach are found to be in agreement with previous studies, provided that the seismic input is adapted to include amplification effects.

Keywords Retaining walls · Pseudo-dynamic analysis · Active earth pressure · Earthquakes

I. Bellezza (✉)
Department of SIMAU, Università Politecnica delle Marche, Ancona, Italy
e-mail: i.bellezza@univpm.it

List of symbols

$a_h(z,t)$, $a_v(z,t)$	Horizontal and vertical acceleration in the backfill at depth z and time t
a_{h0}, a_{v0}	Amplitude of horizontal and vertical acceleration at the base of the wall
$a_{h,max}$, $a_{v,max}$	Maximum amplitude of horizontal and vertical acceleration at the ground surface
$a_{h,avg}$, $a_{v,avg}$	Weighted average horizontal and vertical acceleration within soil wedge
$a_{h,avg,max}$, $a_{v,avg,max}$	Maximum values of $a_{h,avg}$ and $a_{v,avg}$
A_h, B_h, A_v, B_v	Numerical coefficients for horizontal and vertical inertia force
A_{mh}, B_{mh} A_{mv}, B_{mv}	Numerical coefficients for overturning moment
A_{ph}, B_{pz} A_{pv}, B_{pv}	Numerical coefficients for seismic active pressure

D_s	Damping ratio for *S*-wave
D_p	Damping ratio for *P*-wave
D	Generic damping ratio
E_c	Constrained modulus of soil $=\lambda + 2G$
f_{ah}, f_{av}	Ratio between amplitude of horizontal (vertical) acceleration at the ground surface and at the base of the layer
g	Acceleration due to gravity
G	Shear modulus of the soil
H	Height of wall and soil layer
h_P	Distance of the point of application of $P_{AE,max}$ from the wall base
K_{AE}	Active earth pressure coefficient in the pseudo-dynamic approach
M	Overturning moment with respect to the base of the wall
$p_{ae}(z, \alpha, t)$	Total seismic active pressure
$P_{AE}(\alpha, t)$	Generic value for active thrust in the pseudo-dynamic approach
$P_{AE,max}$	Maximum value of P_{AE}
Q_h	Horizontal inertia force of the soil wedge
Q_v	Vertical inertia force of the soil wedge
$Q_{h,max}$	Maximum value of Q_h
$Q_{v,max}$	Maximum value of Q_v
R	Resultant of soil force acting on the failure plane
T_s	Period of the harmonic base horizontal acceleration and horizontal inertia force Q_h
T_p	Period of the harmonic vertical acceleration and vertical inertia force Q_v
T_{sp}	Period of P_{AE}
t	Time
t_m	Time at which P_{AE} is maximum
u_h, u_v	Horizontal and vertical soil displacement
V_S, V_P	Velocity of *P*-waves and *S*-waves in the soil
W	Weight of the soil wedge
y_{s1}, y_{s2}	Adimensional factors governing horizontal acceleration
y_{p1}, y_{p2}	Adimensional factors governing vertical acceleration
z	Depth from the top of the backfill
z_n	z/H
α	Inclination of the soil wedge with respect to the horizontal plane
α_m	Value of α which maximizes P_{AE}
δ	Friction angle between backfill and wall
φ	Shear resistance angle of the backfill
ε_{ij}	Generic strain
γ	Unit weight of soil
η_s, η_1, η_p	Viscosities of the soil
λ	First Lamé constant
ρ	Soil density
σ_{ij}	Generic stress
ω_s	Angular frequency of motion for *S*-wave
ω_p	Angular frequency of motion for *P*-wave

1 Introduction

Design of retaining walls under seismic conditions is a very important topic in geotechnical engineering.

Among various approaches available the finite element methods coupled with advanced constitutive models allow to well describe the complex dynamic behavior of geo-structures. However the use of such sophisticated methods requires both a proper selection of several parameters and a specific knowledge of earthquake geotechnical engineering that is not so commonly diffused in technical community.

In current practice simplified methods are still used in which seismic analysis of retaining walls is obtained as a function of few parameters relatively easy to estimate. The most popular simplified method is the pseudo-static method or Mononobe–Okabe method, developed in the 1920s as an extension of the static Coulomb theory (Okabe 1926; Mononobe and Matsuo

1929). It is widely recognized that a pseudo-static analysis considers the dynamic nature of earthquakes in a very approximate manner and does not account for the effects of time.

To overcome this drawback Steedman and Zeng (1990) proposed a simple pseudo-dynamic analysis of seismic active earth thrust that incorporates phase difference and amplification effects in a dry elastic backfill behind a vertical retaining wall subjected only to horizontal acceleration that varies along the face of the wall. Further improvements of the original pseudo-dynamic method were proposed in the literature in order to consider vertical acceleration, non vertical walls, inclined or submerged backfill (Choudhury and Nimbalkar 2006; Ghosh 2008, 2010; Kolathayar and Ghosh 2009; Bellezza et al. 2012).

The pioneering pseudo-dynamic method was also extended to passive case (Choudhury and Nimbalkar 2005; Ghosh 2007; Ghosh and Kolathayar 2011). The same framework was utilized to estimate seismic displacements (Choudhury and Nimbalkar 2007, 2008) and to design retaining structures also with reinforced backfill (Nimbalkar et al. 2006; Nimbalkar and Choudhury 2007; Choudhury and Ahmad 2008; Ahmad and Choudhury 2008a, b, 2009).

Despite its various applications, a careful review of the original pseudo-dynamic method highlighted some critical aspects; in particular it considers only incident waves travelling upward throughout a linear elastic backfill, resulting in a violation of the free-surface boundary condition (Bellezza et al. 2012, 2014; Choudhury et al. 2014a, b).

Recently in the literature various approaches have been presented to overcome this shortcoming. Some studies considered Rayleigh waves to calculate both active and passive earth pressure on retaining walls (Choudhury and Katdare 2013; Choudhury et al. 2014a).

Bellezza (2014) proposed a new pseudo-dynamic approach based on a standing shear wave in a visco-elastic backfill overlying a rigid base subject to harmonic shaking. Maintaining other hypotheses of the existing pseudo-dynamic method—including absence of water, homogeneous backfill and planar failure surface—closed form expressions for the horizontal inertia force, seismic active thrust, active pressure distribution and overturning moment were derived in dimensionless form as a function of the normalized frequency of shear wave and damping ratio.

In this paper a more complete study is presented in which the seismic active thrust is obtained including also the vertical acceleration. Unlike the pioneering pseudo-dynamic approach a different angular frequency for S-wave and P-wave is accounted for.

2 Wave Equation for a Visco-Elastic Soil

For the purposes of viscoelastic wave propagation, soils are usually modeled as Kelvin–Voigt materials represented by a purely elastic spring and a purely viscous dashpot connected in parallel (Kramer 1996). The same model is also used by ASTM D4015 (2007) to analyze resonant column test results.

The constitutive equation of the Kelvin–Voigt visco-elastic medium is given by:

$$\sigma_{ij} = 2G\varepsilon_{ij} + 2\eta \frac{\partial \varepsilon_{ij}}{\partial t} \tag{1}$$

where σ_{ij} is a stress ε_{ij} is a strain G is the shear modulus and η is a viscosity.

The motion equation of the Kelvin–Voigt visco-elastic medium can be written in vectorial form as (see for example Yuan et al. 2006):

$$\rho \frac{\partial^2 \mathbf{u}}{\partial t^2} = \left\{ (\lambda + G) + (\eta_1 + \eta_s) \frac{\partial}{\partial t} \right\} grad(\theta) + \left(G + \eta_s \frac{\partial}{\partial t} \right) \nabla^2 \mathbf{u} \tag{2}$$

where ρ is the density of the material, λ and G are the Lamè constant, η_1 and η_s are viscosities, $\mathbf{u}$ is the displacement vector of components u_x, u_y and u_z and $\theta = div(\mathbf{u})$.

If the plane wave solution of a wave propagating along the z-axis in a Kelvin–Voigt homogeneous medium is considered, then (2) can be simplified as:

$$\rho \frac{\partial^2 u_h}{\partial t^2} = G \frac{\partial^2 u_h}{\partial z^2} + \eta_s \frac{\partial^3 u_h}{\partial t \partial z^2} \tag{3}$$

$$\rho \frac{\partial^2 u_v}{\partial t^2} = (\lambda + 2G) \frac{\partial^2 u_v}{\partial z^2} + (\eta_1 + 2\eta_s) \frac{\partial^3 u_v}{\partial t \partial z^2} \tag{4}$$

where $u_h = u_x$ and $u_v = u_z$.

2.1 Horizontal Displacement and Acceleration

For a harmonic horizontal base shaking of angular frequency ω_s and period T_s (=$2\pi/\omega_s$) the solution of (3) is obtained by Bellezza (2014) as a function of damping ratio D_s (=$\eta_s\omega_s/2G$) and normalized frequency of S-wave ($\omega_s H/V_s$). Assuming a base displacement $u_{bh} = u_{h0}\cos(\omega_s t)$ the horizontal displacement within a layer of thickness H is given by:

$$u_h(z,t) = \frac{u_{h0}}{C_S^2 + S_S^2}[(C_S C_{sz} + S_S S_{sz})\cos(\omega_s t) + (S_S C_{sz} - C_S S_{sz})\sin(\omega_s t)] \tag{5}$$

Defining $a_{h0} = -\omega_s^2 u_{h0}$, the horizontal acceleration is easily obtained as:

$$a_h(z,t) = \frac{a_{h0}}{C_S^2 + S_S^2}[(C_S C_{sz} + S_S S_{sz})\cos(\omega_s t) + (S_S C_{sz} - C_S S_{sz})\sin(\omega_s t)] \tag{6}$$

where:

$$C_{sz} = \cos(y_{S1}z/H)\cosh(y_{S2}z/H) \tag{7a}$$

$$S_{sz} = -\sin(y_{S1}z/H)\sinh(y_{S2}z/H) \tag{7b}$$

$$C_S = \cos(y_{S1})\cosh(y_{S2}) \tag{7c}$$

$$S_S = -\sin(y_{S1})\sinh(y_{S2}) \tag{7d}$$

$$y_{S1} = k_{s1}H = \frac{\omega_s H}{V_s}\sqrt{\frac{\sqrt{1+4D_s^2}+1}{2(1+4D_s^2)}} = \frac{\omega_s H}{\sqrt{G/\rho}}\sqrt{\frac{\sqrt{1+4D_s^2}+1}{2(1+4D_s^2)}} \tag{8a}$$

$$y_{S2} = k_{s2}H = -\frac{\omega_s H}{V_s}\sqrt{\frac{\sqrt{1+4D_s^2}-1}{2(1+4D_s^2)}} = -\frac{\omega_s H}{\sqrt{G/\rho}}\sqrt{\frac{\sqrt{1+4D_s^2}-1}{2(1+4D_s^2)}} \tag{8b}$$

where k_{s1} and k_{s2} are the real and imaginary part of the complex wave number k_s^*, defined as a function of the complex shear modulus G^*; in particular $k_s^* = \omega_s\sqrt{\rho/G^*} = k_{s1} + ik_{s2}$ and $G^* = G(1 + 2iD_s)$. Further details about the complex wave number and complex shear modulus appear in many text books (e.g. Kolsky 1963; Kramer 1996).

2.2 Vertical Displacement and Acceleration

Equation (4) can be written in a form similar to Eq. (3) provided that u_h, G and η_s are replaced by u_v, E_c (=$\lambda + 2G$) and $\eta_p = (\eta_1 + 2\eta_s)$, respectively.

Considering a harmonic vertical shaking of the base $u_{vb} = u_{v0}\cos(\omega_p t)$and by imposing that at the free surface ($z = 0$) the normal stress is null ($\sigma_{zz} = 0$) and that at $z = H$ the displacement coincides with that of the rigid base, the solution of (4) can be expressed as a function of damping ratio D_p (=$\eta_p\omega_p/2E_c$) and normalized frequency of P-wave ($\omega_p H/V_p$). Then, the vertical displacement within a layer of thickness H can be calculated as:

$$u_v(z,t) = \frac{u_{v0}}{C_P^2 + S_P^2}\left[\left(C_P C_{pz} + S_P S_{pz}\right)\cos\left(\omega_p t\right) + \left(S_P C_{pz} - C_P S_{pz}\right)\sin\left(\omega_p t\right)\right] \tag{9}$$

Defining $a_{v0} = -\omega_p^2 u_{v0}$, the vertical acceleration is given by:

$$a_v(z,t) = \frac{a_{v0}}{C_P^2 + S_P^2}\left[\left(C_P C_{pz} + S_P S_{pz}\right)\cos\left(\omega_p t\right) + \left(S_P C_{pz} - C_P S_{pz}\right)\sin\left(\omega_p t\right)\right] \tag{10}$$

where:

$$C_{pz} = \cos\left(y_{p1}z/H\right)\cosh\left(y_{p2}z/H\right) \tag{11a}$$

$$S_{pz} = -\sin\left(y_{p1}z/H\right)\sinh\left(y_{p2}z/H\right) \tag{11b}$$

$$C_P = \cos\left(y_{p1}\right)\cosh\left(y_{p2}\right) \tag{11c}$$

$$S_P = -\sin\left(y_{p1}\right)\sinh\left(y_{p2}\right) \tag{11d}$$

$$y_{p1} = \frac{\omega_p H}{V_p}\sqrt{\frac{\sqrt{1+4D_p^2}+1}{2\left(1+4D_p^2\right)}} = \frac{\omega_p H}{\sqrt{E_c/\rho}}\sqrt{\frac{\sqrt{1+4D_p^2}+1}{2\left(1+4D_p^2\right)}} \tag{12a}$$

$$y_{p2} = -\frac{\omega_p H}{V_p}\sqrt{\frac{\sqrt{1+4D_p^2}-1}{2\left(1+4D_p^2\right)}} = -\frac{\omega_p H}{\sqrt{E_c/\rho}}\sqrt{\frac{\sqrt{1+4D_p^2}-1}{2\left(1+4D_p^2\right)}} \tag{12b}$$

It is worthy to note that soil accelerations described by (6) and (10) automatically incorporate amplification effects within the soil layer without introducing an amplification factor as needed in the original pseudo-dynamic approach (Steedman and Zeng 1990; Choudhury and Nimbalkar 2007, 2008; Nimbalkar and Choudhury 2007).

The ratio between the amplitude of horizontal and vertical acceleration at the ground surface and at the base of the layer can be calculated as:

$$f_{ah} = \frac{max\{a_h(z=0,t)\}}{max\{a_h(z=H,t)\}} = \frac{a_{h0}\Big/\sqrt{C_S^2+S_S^2}}{a_{h0}} = \frac{1}{\sqrt{\cos^2 y_{s1} + \operatorname{senh}^2 y_{s2}}} \tag{13}$$

$$f_{av} = \frac{max\{a_v(z=0,t)\}}{max\{a_v(z=H,t)\}} = \frac{a_{v0}\Big/\sqrt{C_P^2+S_P^2}}{a_{v0}} = \frac{1}{\sqrt{\cos^2 y_{p1} + \operatorname{senh}^2 y_{p2}}} \tag{14}$$

3 Pseudo-Dynamic Inertial Forces

Considering a planar surface inclined at an angle α with respect to the horizontal plane (Fig. 1), the mass of a thin element of the wedge at depth z is given by given by:

$$m(z) = \frac{\gamma(H-z)}{g\tan\alpha}\mathrm{d}z \tag{15}$$

where γ is the unit weight of soil.

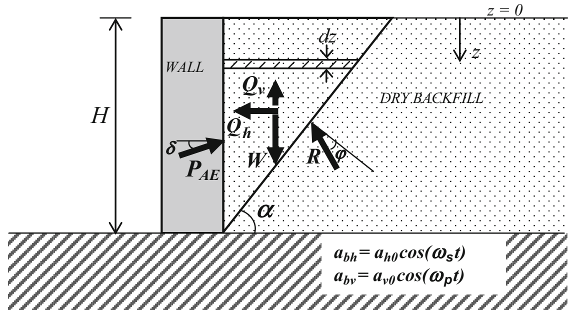

Fig. 1 Scheme of forces acting on soil wedge

$$Q_h(t,\alpha) = \int_{z=0}^{z=H} a_h(z,t)m(z) = \int_{z=0}^{z=H} a_h(z,t)\frac{\gamma(H-z)}{g\tan\alpha}\mathrm{d}z \tag{16}$$

Considering (6), (7) and (8) Bellezza (2014) developed Eq. (16) obtaining:

$$Q_h(t,\alpha) = \frac{a_{h,avg}(t)}{g}W(\alpha)\cdot \tag{17}$$

where W is the weight of soil wedge ($W = 0.5\gamma H^2/\tan\alpha$) and $a_{h,avg}$ is the weighted average horizontal acceleration within the wedge:

$$a_{h,avg} = \frac{1}{0.5H^2/\tan\alpha}\int_0^H \frac{a_h(H-z)}{\tan\alpha}dz = 2a_{h0}[A_h\cos(\omega_s t) + B_h\sin(\omega_s t)] \tag{18}$$

with

$$A_h = \frac{2y_{s1}y_{s2}\sin(y_{s1})\sinh(y_{s2}) + \left(y_{s1}^2 - y_{s2}^2\right)\left\{\cos(y_{s1})\cosh(y_{s2}) - \cos^2(y_{s1}) - \sinh^2(y_{s2})\right\}}{\left(\cos^2(y_{s1}) + \sinh^2(y_{s2})\right)\left(y_{s1}^2 + y_{s2}^2\right)^2} \tag{19a}$$

$$B_h = \frac{2y_{s1}y_{s2}\left\{\cos(y_{s1})\cosh(y_{s2}) - \cos^2(y_{s1}) - \sinh^2(y_{s2})\right\} - \left(y_{s1}^2 - y_{s2}^2\right)\sin(y_{s1})\sinh(y_{s2})}{\left(\cos^2(y_{s1}) + \sinh^2(y_{s2})\right)\left(y_{s1}^2 + y_{s2}^2\right)^2} \tag{19b}$$

The horizontal inertial force of the wedge Q_h, which is assumed to be positive if directed towards the wall, can be calculated as:

Similarly, the vertical inertial force of the wedge Q_v, which is assumed to be positive if directed upward, can be calculated as:

$$Q_v(t,\alpha) = \int\limits_{z=0}^{z=H} a_v(z,t)m(z) = \int\limits_{z=0}^{z=H} a_v(z,t)\frac{\gamma(H-z)}{g\tan\alpha}dz \tag{20}$$

After substituting (10) into (20) and solving the integral, Q_v can be written in a form similar to (17):

$$Q_v(t,\alpha) = \frac{a_{v,avg}(t)}{g}W(\alpha) \tag{21}$$

where $a_{v,avg}$ is the weighted average vertical acceleration within the wedge:

$$\begin{aligned} a_{v,avg} &= \frac{1}{0.5H^2/\tan\alpha}\int\limits_0^H \frac{a_v(H-z)}{\tan\alpha}dz \\ &= 2a_{v0}\left[A_v\cos(\omega_p t) + B_v\sin(\omega_p t)\right] \end{aligned} \tag{22}$$

and A_v and B_v are dimensionless coefficients dependent on y_{p1} and y_{p2}:

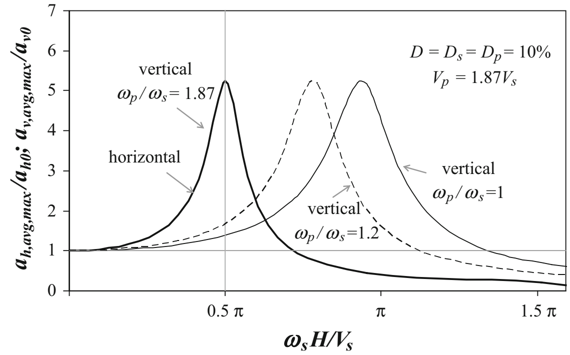

Fig. 2 Influence of normalized frequency of S-wave on maximum weighted average accelerations within the soil wedge for $D = 10$ %

$D = D_s = D_p = 10$ % assuming $V_p/V_s = 1.87$. This latter hypothesis is generally accepted in the literature for dry soils (Das 1993; Kramer 1996) and it occurs when Poisson's ratio is equal to 0.3.

$$A_v = \frac{2y_{p1}y_{p2}\sin(y_{p1})\sinh(y_{p2}) + \left(y_{p1}^2 - y_{p2}^2\right)\left\{\cos(y_{p1})\cosh(y_{p2}) - \cos^2(y_{p1}) - \sinh^2(y_{p2})\right\}}{\left(\cos^2(y_{p1}) + \sinh^2(y_{p2})\right)\left(y_{p1}^2 + y_{p2}^2\right)^2} \tag{23a}$$

$$B_v = \frac{2y_{p1}y_{p2}\left\{\cos(y_{p1})\cosh(y_{p2}) - \cos^2(y_{p1}) - \sinh^2(y_{p2})\right\} - \left(y_{p1}^2 - y_{p2}^2\right)\sin(y_{p1})\sinh(y_{p2})}{\left(\cos^2(y_{p1}) + \sinh^2(y_{p2})\right)\left(y_{p1}^2 + y_{p2}^2\right)^2} \tag{23b}$$

It is easy to demonstrate that the maximum values of $a_{h,avg}$ and $a_{v,avg}$ are given by:

$$a_{h,avg,max} = 2|a_{h0}|\sqrt{A_h^2 + B_h^2} \tag{24}$$

$$a_{v,avg,max} = 2|a_{v0}|\sqrt{A_v^2 + B_v^2} \tag{25}$$

Equations (24) and (25) indicate that $a_{h,avg,\max}$ and $a_{v,avg,\max}$ depend on the normalized frequency ($\omega_s H/V_s$ and $\omega_p H/V_p$) and damping ratio (D_s and D_p) as well as the amplitudes of base accelerations a_{h0} and a_{v0}.

In Fig. 2 values of the ratios $a_{h,avg,max}/a_{h0}$ and $a_{v,avg,max}/a_{v0}$ are plotted against the normalized frequency of the S-wave ($\omega_s H/V_s$) for

It is evident that all curves of Fig. 2 show a similar trend with the same maximum value which depends on damping ratio; the curves are shifted as the maximum average horizontal acceleration peaks when the S-wave reaches its fundamental frequency ($\omega_s H/V_s = \pi/2$) whereas the P-wave peaks for $\omega_p H/V_p = \pi/2$, at which corresponds $\omega_s H/V_s = \pi/2(V_p/V_s)(\omega_s/\omega_p)$. It can be observed that for $\omega_p/\omega_s > 1$ the curve of the vertical acceleration tends to move left-hand with a complete superimposition to the curve relevant to horizontal acceleration for $\omega_p = 1.87\ \omega_s$.

For a rigid soil (i.e. for $V_s \to \infty$ $V_p \to \infty$) the ratios $a_{h,avg,max}/a_{h0}$ and $a_{v,avg,max}/a_{v0}$ tend to the unit (i.e. $A_h = A_v = 0.5$ $B_v = B_h = 0$).

For values of normalized frequencies ($\omega_s H/V_s$ and $\omega_p H/V_p$) less than the fundamental frequencies the ratios $a_{h,avg,max}/a_{h0}$ and $a_{v,avg,max}/a_{v0}$ are always greater than the unit. In this range soil accelerations are in phase at all depth of soil layer and this results in a significant increase in $a_{h,avg}$ and $a_{v,avg}$.

After the peak for increasing values of normalized frequencies part of the wedge can be subjected to an acceleration in one direction while the other one part can accelerate in the opposite direction and this results in a reduction of the average acceleration of the soil wedge with values of the ratios $a_{h,avg,max}/a_{h0}$ and $a_{v,avg,max}/a_{v0}$ even less than the unity.

Equations (18) and (22) indicate that $a_{h,avg}$ and $a_{v,avg}$ follow a harmonic trend of period T_s and T_p, respectively. Consequently, for an assigned angle α, also the inertial forces Q_h and Q_v calculated by (17) and (21) follow the same trend versus time. Considering (18), (22), (24) and (25) the following expressions hold:

$$\frac{Q_h(t)}{Q_{h,max}} = \frac{a_{h,avg}(t)}{a_{h,avg,max}} = \frac{a_{h0}[A_h\cos(\omega_s t) + B_h\sin(\omega_s t)]}{|a_{h0}|\sqrt{A_h^2 + B_h^2}} \tag{26}$$

$$\frac{Q_v(t)}{Q_{v,max}} = \frac{a_{v,avg}(t)}{a_{v,avg,max}} = \frac{a_{v0}\{A_v\cos(\omega_p t) + B_v\sin(\omega_p t)\}}{|a_{v0}|\sqrt{A_v^2 + B_v^2}} \tag{27}$$

Figure 3 shows an example of the trend versus time of the ratios $Q_h/Q_{h,max}$ and $Q_v/Q_{v,max}$ obtained for $a_{h0} > 0$; $\omega_s H/V_s = 2$; $D = D_s = D_p = 10\ \%$; $\omega_p/\omega_s = 1$. The ratio $Q_v/Q_{v,max}$ is calculated by assuming both positive and negative value of a_{v0}. It is clear that Q_h and Q_v peak at a different times; the time at which the inertia forces reach their maximum depends on the values of normalized frequency ($\omega_s H/V_s$ and $\omega_p H/V_p$) and damping ratio (D_S and D_p). Complete expressions to calculate the time at which Q_h is maximum are provided by Bellezza (2014). Similar expressions can be derived for the vertical inertial force Q_v.

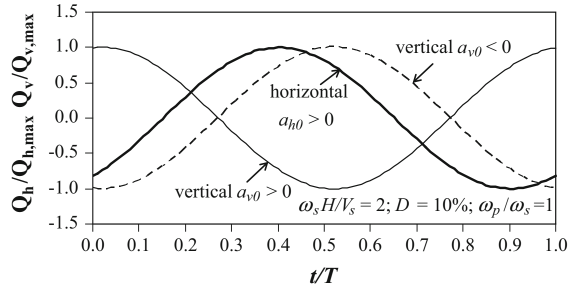

Fig. 3 Example of trend of normalized inertia forces in the period of shaking for $D = 10\ \%$; $\omega_s H/V_s = 2$; $\omega_p/\omega_s = 1$

4 Pseudo-Dynamic Active Thrust

By assuming that the dry cohesionless soil is in the limit condition along the planar failure plane (Fig. 1) and imposing the vertical and horizontal equilibrium of the wedge, the total (static + dynamic) active thrust P_{AE} can be obtained as:

$$P_{AE}(\alpha, t) = \frac{W\sin(\alpha - \varphi) + Q_h\cos(\alpha - \varphi) - Q_v\sin(\alpha - \varphi)}{\cos(\varphi + \delta - \alpha)} \tag{28}$$

where W = weight of the wedge, φ = backfill shear resistance angle; δ = friction angle between the wall and backfill.

The active thrust is taken as the maximum value of P_{AE} with respect to α and t.

Substituting (17) and (21) into (28) gives:

$$\frac{P_{AE,max}}{\gamma H^2} = max\left\{\begin{array}{l} \dfrac{\sin(\alpha-\varphi)}{2\tan\alpha\cos(\varphi+\delta-\alpha)} + \dfrac{\cos(\alpha-\varphi)}{\tan\alpha\cos(\varphi+\delta-\alpha)}\dfrac{a_{h0}}{g}[A_h\cos(\omega_s t) + B_h\sin(\omega_s t)] \\ -\dfrac{\sin(\alpha-\varphi)}{\tan\alpha\cos(\varphi+\delta-\alpha)}\dfrac{a_{v0}}{g}[A_v\cos(\omega_p t) + B_v\sin(\omega_p t)] \end{array}\right\} \tag{29}$$

Similarly to Steedman and Zeng (1990) and Choudhury and Nimbalkar (2006), it is possible to define a pseudo-dynamic coefficient of active thrust:

$$K_{AE} = \frac{2P_{AE,max}}{\gamma H^2} = \frac{\sin(\alpha_m - \varphi)}{\tan\alpha_m \cos(\varphi + \delta - \alpha_m)} + \frac{2\cos(\alpha_m - \varphi)}{\tan\alpha_m \cos(\varphi + \delta - \alpha_m)} \frac{a_{h0}}{g} [A_h \cos(\omega_s t_m) + B_h \sin(\omega_s t_m)] - \frac{2\sin(\alpha_m - \varphi)}{\tan\alpha_m \cos(\varphi + \delta - \alpha_m)} \frac{a_{v0}}{g} [A_v \cos(\omega_p t_m) + B_v \sin(\omega_p t_m)] \tag{30}$$

where α_m and t_m are the values of α and t that maximize K_{AE}. In this study the values of K_{AE} are obtained by an optimization procedure in which the magnitudes of the variables α and t/T_s have been varied independently at an interval of 0.1° and 0.01, respectively.

The value of t_m depends on various factors including α_m, φ, ω_s, ω_p, a_{ho} and a_{v0}. Moreover it can be observed that the maximum active thrust is generally achieved for a time at which Q_h and Q_v do not reach their maximum values (i.e. $a_{h,avg,tm} < a_{h,avg,max}$ and $a_{v,avg,tm} < a_{v,avg,max}$).

From a mathematical point of view the time t_m is the solution of the following equation:

$$\frac{\partial}{\partial t}\left(\frac{2P_{AE,max}}{\gamma H^2}\right) = \frac{2\cos(\alpha_m - \varphi)}{\tan\alpha_m \cos(\varphi + \delta - \alpha_m)} \times \frac{a_{h0}}{g}[-\omega_s A_h \sin(\omega_s t_m) + \omega_s B_h \cos(\omega_s t_m)] - \frac{2\sin(\alpha_m - \varphi)}{\tan\alpha_m \cos(\varphi + \delta - \alpha_m)} \frac{a_{v0}}{g}[-\omega_p A_v \sin(\omega_p t_m) + \omega_p B_v \cos(\omega_p t_m)] = 0 \tag{31}$$

A closed form expression for the time t_m is derived only for $\omega_p = \omega_s = \omega$, i.e. when S-wave and P-wave have the same period $T = T_s = T_p$. In this case Eq. (31) can be written in a simplified form:

$$(A_h - \beta A_v)\tan(\omega t_m) = B_h - \beta B_v \tag{32}$$

where $\beta = \tan(\alpha_m - \varphi)a_{v0}/a_{h0}$.

For $a_{h0} > 0$ the solution of (32) that maximizes K_{AE} is given by:

$$\left(\frac{t_m}{T}\right) = \frac{1}{2\pi}\arctan\frac{B_h - \beta B_v}{A_h - \beta A_v} \quad \text{for } A_h - \beta A_v > 0 \text{ and } B_h - \beta B_v > 0 \tag{33a}$$

$$\left(\frac{t_m}{T}\right) = 1 + \frac{1}{2\pi}\arctan\frac{B_h - \beta B_v}{A_h - \beta A_v} \quad \text{for } A_h - \beta A_v > 0 \text{ and } B_h - \beta B_v < 0 \tag{33b}$$

$$\left(\frac{t_m}{T}\right) = \frac{1}{2\pi}\arctan\frac{B_h - \beta B_v}{A_h - \beta A_v} + \frac{1}{2} \quad \text{for } A_h - \beta A_v < 0 \tag{33c}$$

5 Soil Active Pressure Distribution

It is well known that Coulomb approach does not directly provide the distribution of soil active pressures. However, the seismic active earth pressure distribution can be obtained by writing P_{AE} for a generic z instead of H and then differentiating P_{AE} with respect to z (e.g. Steedman and Zeng 1990; Choudhury and Nimbalkar 2006; Ghosh 2010; Bellezza et al. 2012; Bellezza 2014):

$$p_{ae}(\alpha, t, z) = \frac{\partial P_{AE}}{\partial z} = \frac{\partial}{\partial z}\left\{\frac{W(\alpha, z)\sin(\alpha - \varphi) + Q_h(\alpha, t, z)\cos(\alpha - \varphi) - Q_v(\alpha, t, z)\sin(\alpha - \varphi)}{\cos(\varphi + \delta - \alpha)}\right\} \tag{34}$$

where:

$$W(\alpha, z) = \frac{\gamma z^2}{2\tan\alpha} \tag{35}$$

$$Q_h(\alpha, t, z) = \int_{\zeta=0}^{\zeta=z} a_h(\zeta, t)\frac{\gamma(z - \zeta)}{g\tan\alpha}\mathrm{d}\zeta = \frac{\gamma}{g\tan\alpha}\int_{\zeta=0}^{\zeta=z} a_h(\zeta, t)(z - \zeta)\mathrm{d}\zeta \tag{36}$$

$$Q_V(\alpha, t, z) = \int_{\zeta=0}^{\zeta=z} a_v(\zeta, t)\frac{\gamma(z - \zeta)}{g\tan\alpha}\mathrm{d}\zeta = \frac{\gamma}{g\tan\alpha}\int_{\zeta=0}^{\zeta=z} a_v(\zeta, t)(z - \zeta)\mathrm{d}\zeta \tag{37}$$

Developing (34) taking into account of (35)–(37) the seismic active soil pressure can be expressed in a normalized form as a function of the normalized depth z_n ($z_n = z/H$):

$$\begin{aligned}\frac{p_{ae}}{\gamma H} = {} & \frac{\sin(\alpha-\phi)}{\tan\alpha\cos(\phi+\delta-\alpha)} z_n \\ & + \frac{\cos(\alpha-\phi)}{\tan\alpha\cos(\phi+\delta-\alpha)} \frac{a_{h0}}{g} \left[A_{ph}\cos(\omega_s t)\right. \\ & \left.+ B_{ph}\sin(\omega_s t)\right] \\ & - \frac{\sin(\alpha-\phi)}{\tan\alpha\cos(\phi+\delta-\alpha)} \frac{a_{v0}}{g} \left[A_{pv}\cos(\omega_p t)\right. \\ & \left.+ B_{pv}\sin(\omega_p t)\right]\end{aligned} \tag{38}$$

where:

$$A_{ph} = \frac{(C_S y_{s2} + S_S y_{s1})\cos(y_{s1}z_n)\sinh(y_{s2}z_n) + (C_S y_{s1} - S_S y_{s2})\sin(y_{s1}z_n)\cosh(y_{s2}z_n)}{\left(C_S^2 + S_S^2\right)\left(y_{s1}^2 + y_{s2}^2\right)} \tag{39a}$$

$$B_{ph} = \frac{(S_S y_{s2} - C_S y_{s1})\cos(y_{s1}z_n)\sinh(y_{s2}z_n) + (S_S y_{s1} + C_S y_{s2})\sin(y_{s1}z_n)\cosh(y_{s2}z_n)}{\left(C_S^2 + S_S^2\right)\left(y_{s1}^2 + y_{s2}^2\right)} \tag{39b}$$

$$A_{pv} = \frac{(C_p y_{p2} + S_p y_{p1})\cos(y_{p1}z_n)\sinh(y_{p2}z_n) + (C_p y_{p1} - S_p y_{p2})\sin(y_{p1}z_n)\cosh(y_{p2}z_n)}{\left(C_p^2 + S_p^2\right)\left(y_{p1}^2 + y_{p2}^2\right)} \tag{40a}$$

$$B_{pv} = \frac{(S_p y_{p2} - C_p y_{p1})\cos(y_{p1}z_n)\sinh(y_{p2}z_n) + (S_p y_{p1} + C_p y_{p2})\sin(y_{p1}z_n)\cosh(y_{p2}z_n)}{\left(C_p^2 + S_p^2\right)\left(y_{p1}^2 + y_{p2}^2\right)} \tag{40b}$$

The distribution of active soil pressure described by (38)–(40) is clearly non-linear.

The total seismic pressure p_{ae} can be viewed as the sum of three components, the first one is independent of seismic accelerations, the second and third dependent on the horizontal and vertical acceleration, respectively.

The first component, although independent of a_{ho} and a_{v0}, does not represent the active pressure in static conditions (i.e. for $a_{h0} = a_{v0} = 0$) because the value of α_m in static conditions is greater than α_m in seismic conditions.

The point of application (h_p) of total seismic active thrust can be calculated on the basis of the overturning moment respect to the wall base:

$$h_P = \frac{M}{P_{AE}\cos\delta} = \frac{\int_{z=0}^{z=H} p_{ae}\cos\delta(H-z)\mathrm{d}z}{0.5K_{AE}\gamma H^2\cos\delta} \tag{41}$$

After substituting (38) into (41) and solving the integral the normalized point of application is given by:

$$\frac{h_P}{H} = \frac{M/\gamma H^3}{0.5K_{AE}\cos\delta} \tag{42}$$

where

$$\frac{M}{\gamma H^3} = \frac{\cos\delta}{\tan\alpha\,\cos(\phi+\delta-\alpha)} \left\{ \begin{aligned} & \frac{1}{6}\sin(\alpha-\phi) + \cos(\alpha-\phi)\frac{a_{h0}}{g}\{A_{mh}\cos(\omega_s t) + B_{mh}\sin(\omega_s t)\} \\ & -\sin(\alpha-\phi)\frac{a_{v0}}{g}\{A_{mv}\cos(\omega_p t) + B_{mv}\sin(\omega_p t)\} \end{aligned} \right\} \tag{43}$$

$$A_{mh} = \int_0^1 A_{ph}(1-z_n)\mathrm{d}z_n = \frac{\begin{bmatrix} \left(y_{s2}^3 - 3y_{s1}^2 y_{s2}\right)\sinh(y_{s2})\cosh(y_{s2}) + \left(3y_{s1}y_{s2}^2 - y_{s1}^3\right)\sin(y_{s1})\cos(y_{s1}) \\ +2y_{s1}y_{s2}\left(y_{s1}^2 + y_{s2}^2\right)\sin(y_{s1})\sinh(y_{s2}) + \left(y_{s1}^4 - y_{s2}^4\right)\cos(y_{s1})\cosh(y_{s2}) \end{bmatrix}}{\left(\cos^2(y_{s1}) + \sinh^2(y_{s2})\right)\left(y_{s1}^2 + y_{s2}^2\right)^3} \tag{44a}$$

$$B_{mh} = \int_0^1 B_{ph}(1-z_n)\mathrm{d}z_n = \frac{\begin{bmatrix} \left(y_{s1}^3 - 3y_{s1}y_{s2}^2\right)\sinh(y_{s2})\cosh(y_{s2}) + \left(y_{s2}^3 - 3y_{s1}^2 y_{s2}\right)\sin(y_{s1})\cos(y_{s1}) \\ -\left(y_{s1}^4 - y_{s2}^4\right)\sin(y_{s1})\sinh(y_{s2}) + 2y_{s1}y_{s2}\left(y_{s1}^2 + y_{s2}^2\right)\cos(y_{s1})\cosh(y_{s2}) \end{bmatrix}}{\left(\cos^2(y_{s1}) + \sinh^2(y_{s2})\right)\left(y_{s1}^2 + y_{s2}^2\right)^3} \tag{44b}$$

$$A_{mv} = \int_0^1 A_{pv}(1-z_n)\mathrm{d}z_n = \frac{\begin{bmatrix} \left(y_{p2}^3 - 3y_{p1}^2 y_{p2}\right)\sinh(y_{p2})\cosh(y_{p2}) + \left(3y_{p1}y_{p2}^2 - y_{p1}^3\right)\sin(y_{p1})\cos(y_{p1}) \\ +2y_{p1}y_{p2}\left(y_{p1}^2 + y_{p2}^2\right)\sin(y_{p1})\sinh(y_{p2}) + \left(y_{p1}^4 - y_{p2}^4\right)\cos(y_{p1})\cosh(y_{p2}) \end{bmatrix}}{\left(\cos^2(y_{p1}) + \sinh^2(y_{p2})\right)\left(y_{p1}^2 + y_{p2}^2\right)^3} \tag{45a}$$

$$B_{mv} = \int_0^1 B_{pv}(1-z_n)\mathrm{d}z_n = \frac{\begin{bmatrix} \left(y_{p1}^3 - 3y_{p1}y_{p2}^2\right)\sinh(y_{p2})\cosh(y_{p2}) + \left(y_{p2}^3 - 3y_{p1}^2 y_{p2}\right)\sin(y_{p1})\cos(y_{p1}) \\ -\left(y_{p1}^4 - y_{p2}^4\right)\sin(y_{p1})\sinh(y_{p2}) + 2y_{p1}y_{p2}\left(y_{p1}^2 + y_{p2}^2\right)\cos(y_{p1})\cosh(y_{p2}) \end{bmatrix}}{\left(\cos^2(y_{p1}) + \sinh^2(y_{p2})\right)\left(y_{p1}^2 + y_{p2}^2\right)^3} \tag{45b}$$

The angle α in (43) is the same one (α_m) that maximizes the active thrust P_{AE}, as the uniqueness of the planar failure surface in seismic conditions is assumed (i.e. the failure surface, once formed, does not change thereafter).

As noted by Bellezza (2014) the maximum overturning moment is reached at a slightly different time to when the active thrust is maximum; in other words, the soil pressure distribution which gives the maximum soil thrust does not exactly coincide with that producing the maximum moment. However, the difference between the maximum overturning moment and the moment produced by P_{AE} is found to be very small and negligible for practical purposes.

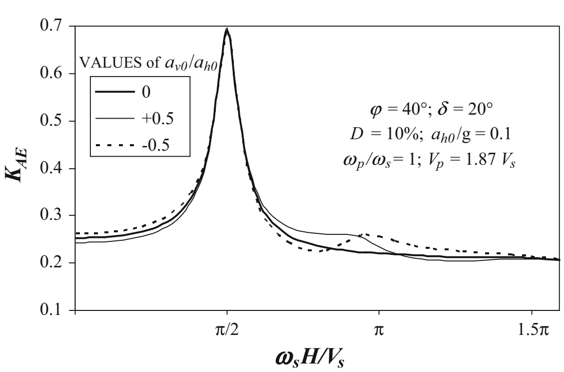

Fig. 4 Influence of the vertical acceleration and normalized frequency of S-wave on seismic active soil coefficient K_{AE} for $\varphi = 40°$; $\delta = 20°$; $a_{h0}/g = 0.1$; $D = 10\ \%$; $\omega_p/\omega_s = 1$

6 Results and Discussion

6.1 Applicability of the Pseudo-Dynamic Method

It is well established (e.g. Okabe 1926; Mononobe and Matsuo 1929; Kramer 1996) that using the traditional pseudo-static approach, for a *vertical* wall retaining a *horizontal* backfill (Fig. 1), the coefficient K_{AE} is given by:

$$K_{AE} = \frac{\cos^2(\varphi - \psi)}{\cos\psi\cos(\delta + \psi)\left[1 + \sqrt{\frac{\sin(\varphi+\delta)\sin(\varphi-\psi)}{\cos(\delta+\psi)}}\right]^2} \tag{46}$$

where $\psi = \arctan(k_h/(1 - k_v))$; k_h = horizontal seismic coefficient. k_v = vertical seismic coefficient.

The inclination of the planar slip surface that maximizes the active thrust can be calculated by a rather complex expression as a function of φ, δ and ψ (e.g. Kramer 1996).

It can be demonstrated that the values of K_{AE} obtained by the pseudo-dynamic method are linked to those obtained by the pseudo-static method. In particular:

$$K_{AE} = K_{AE,ps}\left(1 - a_{v,avg,tm}/g\right) \tag{47}$$

where $K_{AE,ps}$ is the active coefficient calculated by (46) provided $\tan\psi = \frac{a_{h,avg.tm}/g}{\left(1-a_{v,avg.tm}/g\right)}$

The form of (46) indicates that the maximization procedure only yields results if $\varphi > \psi$, i.e. when:

$$\frac{a_{h,avg,tm}/g}{1 - a_{v,avg,tm}/g} \leq \tan\varphi \tag{48}$$

6.2 Effect of Vertical Acceleration

Figure 4 shows the combined effect on K_{AE} of the normalized frequency $\omega_s H/V_s$ and vertical acceleration assuming $D = D_S = D_p = 10\ \%$; $a_{h0} = 0.1$ g; $\varphi = 40°$; $\delta = 20°$; $\omega_p/\omega_s = 1$.

In particular the curve relevant to absence of vertical acceleration ($a_{v0} = 0$) is compared with those obtained for $a_{v0} = 0.5a_{h0}$ and $a_{v\ 0} = -0.5a_{h0}$.

The trend of K_{AE} versus $\omega_s H/V_s$ is not monotonic and two main parts of the curves can be distinguished. For low values of $\omega H/V_s$, K_{AE} sharply increases with $\omega H/V_s$ reaching a local maximum, while in the second part the K_{AE} trend is generally a downwards one, even if a second local maximum of K_{AE} occurs in the presence of the vertical acceleration. The first local maximum of K_{AE} occurs when $\omega_s H/V_s$ is close to $\pi/2$ i.e. when the backfill is subjected to the fundamental frequency of S-wave and the average weighted horizontal acceleration is maximum (see Fig. 2). The second local maximum of K_{AE} occurs when the average weighted vertical acceleration is maximum; this occurs for $\omega_p H/V_p = \pi/2$ at which corresponds $\omega_s H/V_s = 2.93$ in the hypothesis that $V_p = 1.87\ V_s$ and $\omega_p/\omega_s = 1$, as shown in Fig. 2.

For the overall range of $\omega_s H/V_s$, except close to the fundamental frequency, the effect of the vertical acceleration is appreciable; in other words the curves relevant to $a_{v0} \neq 0$ are different to that obtained for $a_{v0} = 0$ and the values of K_{AE} obtained for $a_{v0} > 0$ differ from those obtained for $a_{v0} < 0$.

This difference can be explained with the phase difference between Q_h and Q_v. Provided that the maximum active thrust is achieved when Q_h is close to its maximum, the different sign of a_{v0} implies that when Q_h is close to its positive peak, Q_v can be directed upward or downward (see Fig. 3) and this results in different values of K_{AE}. As explained later, the effect of phase difference between Q_h and Q_v is magnified in the hypothesis that S-wave and P-wave have the same period.

It can be observed that also for a rigid soil ($\omega_s H/V_s \to 0$) the values of K_{AE} are found to be slightly dependent on both value and sign of a_{v0}. As noted previously, the values of K_{AE} obtained by the pseudo-dynamic approach are correlated with those obtained with the pseudo-static method according to (47).

For a rigid soil (47) becomes

$$K_{AE} = K_{AE,ps}(1 - a_{v0}/g). \tag{49}$$

Considering that most technical codes (e.g. Eurocode 8 (2005)) recommend to assume vertical inertia force both upward and downward, in the followings of the paper the value of K_{AE} is assumed as the maximum K_{AE} obtained for $a_{v0} > 0$ and $a_{v0} < 0$. Similarly to the pseudo-static approach (Fang and Chen 1995), it is not assured a priori if the maximum K_{AE} is reached for $a_{v0} > 0$ or for $a_{v0} < 0$. This is evident also in Fig. 4 where for the same input parameters the maximum K_{AE} is obtained for $a_{v0} > 0$ in certain ranges of $\omega_s H/V_s$ and for $a_{v0} < 0$ in other ones.

Figure 5 shows normalized distribution of active seismic pressure for three different value of a_{v0} with $a_{h0}/g = 0.1$; $\omega_s H/V_s = 2$; $\omega_p/\omega_s = 1$; $D = 10\ \%$; $\varphi = 40°$; $\delta = 20°$.

It can be noted that as a_{v0} increases active earth pressure also increases. When a_{v0} changes from 0 to

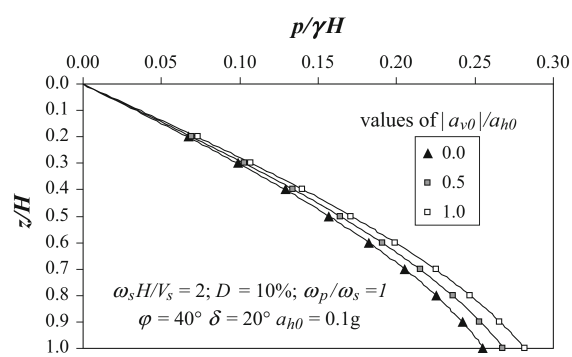

Fig. 5 Normalized seismic active earth pressure distribution for different values of vertical acceleration for $\varphi = 40°$; $\delta = 20°$; $a_{h0}/g = 0.1$; $D = 10\ \%$; $\omega_s H/V_s = 2$; $\omega_p/\omega_s = 1$

$0.5a_{h0}$ seismic active earth thrust increases by about 4.6 %. Similarly when a_{vo} changes from $0.5a_{h0}$ to a_{h0} seismic active earth thrust increases by about 4.7 %.

6.3 Effect of Horizontal Acceleration

Figure 6 shows the typical normalized pressure distribution for different values of a_{h0} with $|a_{vo}| = 0.5a_{h0}$; $\varphi = 40°$; $\delta = 20°$; $\omega_s H/V_s = 2$; $\omega_p/\omega_s = 1$. As expected, it is evident that as a_{h0} increases, seismic active earth pressure also increases. This results in a significant increase in active soil thrust. As an example K_{AE} increases by about 45 % when a_{h0} changes from 0.1 g to 0.2 g.

From Fig. 6 it is also clear that degree of non-linearity of the curves increases with a_{h0}. The point of application of P_{AE} calculated by (42) is found to slightly increase from $0.343H$ for $a_{h0} = 0.05$ g to $0.367H$ for $a_{h0} = 0.20$ g.

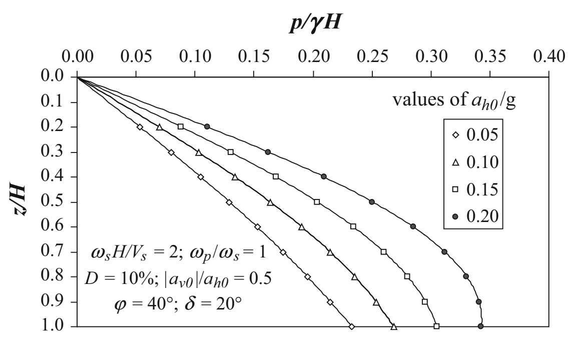

Fig. 6 Normalized seismic active earth pressure distribution for different values of amplitude of base horizontal acceleration for $\varphi = 40°$; $\delta = 20°$; $|a_{v0}|/a_{h0} = 0.5$; $D = 10$ %; $\omega_s H/V_s = 2$; $\omega_p/\omega_s = 1$

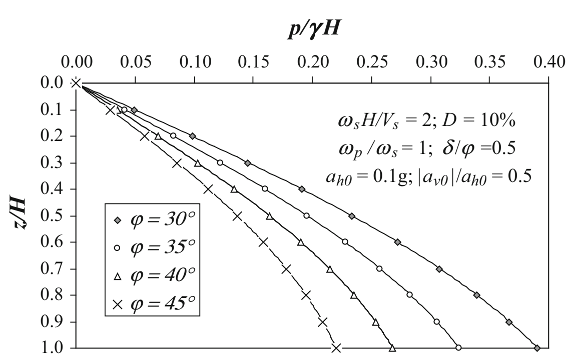

Fig. 7 Normalized seismic active earth pressure distribution for different values of soil shear resistance angle for $\delta/\varphi = 0.5$; $a_{h0}/g = 0.1$; $|a_{v0}|/a_{h0} = 0.5$; $D = 10$ %; $\omega_s H/V_s = 2$; $\omega_p/\omega_s = 1$

6.4 Effect of Soil Shear Resistance Angle and Soil-Wall Friction Angle

Figure 7 shows the normalized pressure distribution for different values of soil shear resistance angle φ with $a_{h0} = 0.1$ g; $|a_{v0}| = 0.5a_{ho}$, $\omega_s H/V_s = 2$; $D = 10$ %; $\delta = \varphi/2$. As expected, seismic active earth pressure shows significant decrease with the increase in the value of φ. When φ changes from 30° to 35° seismic active earth pressure decreases by about 16 % at mid-height and by about 17 % at the bottom of the wall. Similarly when φ changes from 35° to 40° seismic active earth pressure decreases by about 16.3 % at mid-height and by about 17.3 % at the bottom of the wall. Finally when φ changes from 40° to 45° seismic active earth pressure decreases by about 16.7 % at mid-height and by about 17.9 % at the bottom of the wall.

Figure 8 shows the normalized pressure distribution for different values of soil-wall friction angle δ with $a_{h0}/g = 0.1$, $|a_{v0}| = 0.5a_{h0}$, $\omega_s H/V_s = 2$; $D = 10$ %; $\varphi = 40°$. The effect of δ is quite marginal.

For the same input parameters Fig. 9 shows the combined effect on K_{AE} of φ and δ/φ for four different values of φ. It is clear that the effect of δ on K_{AE} is generally small if compared with that of φ. In the investigated ranges of φ ($\varphi = 30°$–$45°$) the trend of K_{AE} versus δ/φ is not monotonic with a minimum value of K_{AE} for δ/φ in the range 0.25–0.50. The maximum value of K_{AE} is reached in most cases for $\delta = \varphi$, except the case of $\varphi = 30°$ when the

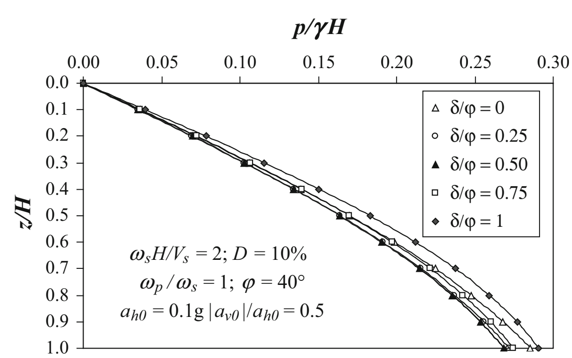

Fig. 8 Normalized seismic active earth pressure distribution for different values of soil wall friction angle for $\varphi = 40°$; $a_{h0}/g = 0.1$; $|a_{v0}|/a_{h0} = 0.5$; $D = 10$ %; $\omega_s H/V_s = 2$; $\omega_p/\omega_s = 1$

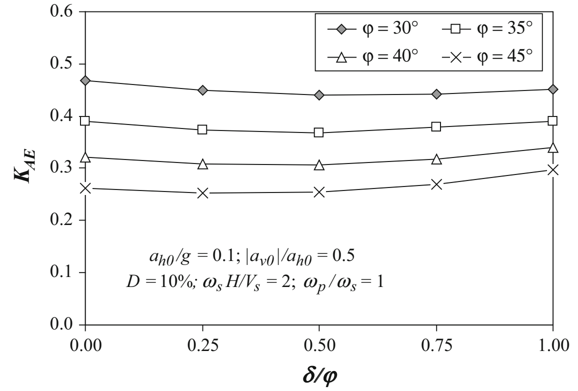

Fig. 9 Effect of wall-backfill friction angle for different values of soil shear resistance angle for $a_{h0}/g = 0.1$; $|a_{v0}|/a_{h0} = 0.5$; $D = 10\ \%$; $\omega_s H/V_s = 2$; $\omega_p/\omega_s = 1$

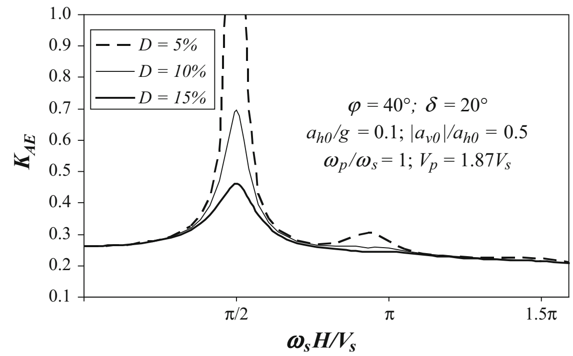

Fig. 10 Effect of damping ratio and normalized frequency of *S*-wave on seismic active soil coefficient K_{AE} for $\varphi = 40°$; $\delta = 20°$; $a_{h0}/g = 0.1$; $|a_{v0}|/a_{h0} = 0.5$; $\omega_s H/V_s = 2$; $\omega_p/\omega_s = 1$

maximum is obtained for $\delta = 0$. The range of variability of K_{AE} is found to increase at increasing φ; the percent difference between the maximum value of K_{AE} and the value obtained for $\delta = \varphi/2$ varies from about 6 % for $\varphi = 30°$ to about 19 % for $\varphi = 45°$.

6.5 Effect of Damping Ratio

The analysis presented in the previous sections allows to consider a different damping ratio for *S*-wave and *P*-wave. However, for a sake of simplicity it is here assumed that $D = D_s = D_p$.

Figure 10 shows the values of K_{AE} at varying $\omega_s H/V_s$ obtained for $D = 5$, 10 and 15 %, all other input parameters being equal ($\varphi = 40°$; $\delta = 20°$; $a_{h0} = 0.1$ g; $|a_{v0}| = 0.5 a_{h0}$). The trend of the three

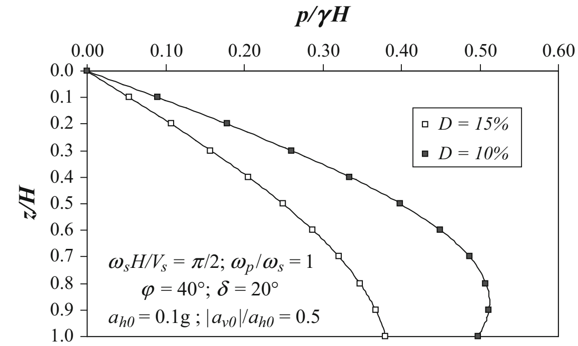

Fig. 11 Normalized seismic active earth pressure distribution for different values of damping ratio for $\varphi = 40°$; $\delta = 20°$; $a_{h0}/g = 0.1$; $|a_{v0}|/a_{h0} = 0.5$; $\omega_s H/V_s = 2$; $\omega_p/\omega_s = 1$

curves is similar with a maximum of K_{AE} when $\omega_s H/V_s$ is close to π/2. For the lower damping ratio ($D = 5\ \%$) the first peak does not exist as the condition expressed by (46) is not satisfied; a second local maximum is found when P-wave reaches its fundamental frequency (i.e. for $\omega_s H/V_s = 2.93$) and a third local maximum is visible when $\omega_s H/V_s$ is close to 1.5π. For $D = 10\ \%$ and $D = 15\ \%$ the second and the third local maxima are not appreciable. In the analyzed case the effect on K_{AE} of soil damping varying in the range 5–15 % is found to be negligible for $\omega_s H/V_s$ ranging between 0 and 1 and very small in the range 3.5–5 in which the values of K_{AE} differ <3.5 %.

On the contrary, the damping ratio is found to have a great effect on the first peak of K_{AE}. For $\omega_s H/V_s = \pi/2$ K_{AE} decreases of about 50 % when D varies from 10–15 %.

Figure 11 shows that a lower damping ratio implies a greater non-linearity of active pressure distribution and a slight rise of the application point of the active thrust ($h_p/H = 0.357$ for $D = 15\ \%$ and $h_p/H = 0.373$ for $D = 10\ \%$).

6.6 Effect of Frequency Ratio

Previous studies based on the original pseudo-dynamic method assumed that angular frequency of S-wave coincide with angular frequency of P-wave (Choudhury and Nimbalkar 2006, 2007, 2008; Nimbalkar and Choudhury 2007, Choudhury and Ahmad 2008; Nimbalkar et al. 2006; Ghosh 2007, 2010; Bellezza et al. 2012). In this study a different frequency for S- and P-wave is considered by the ratio ω_p/ω_s.

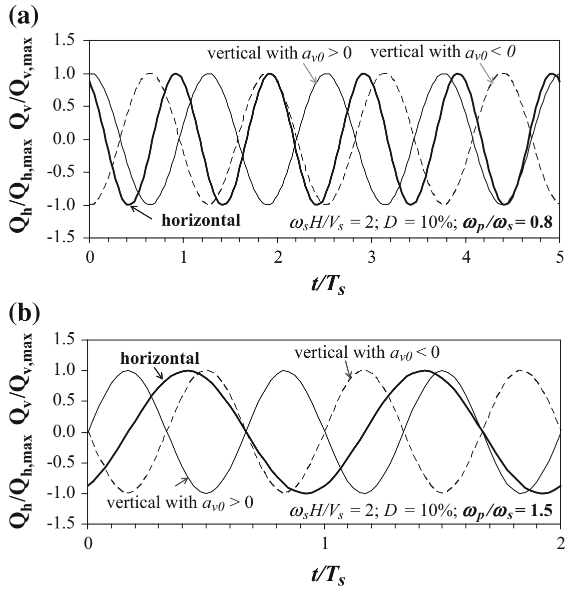

Fig. 12 Normalized values of inertia forces in the overall period for $D = 10\ \%$; $\omega_s H/V_s = 2$ (a) $\omega_p/\omega_s = 0.8$; (b) $\omega_p/\omega_s = 1.5$

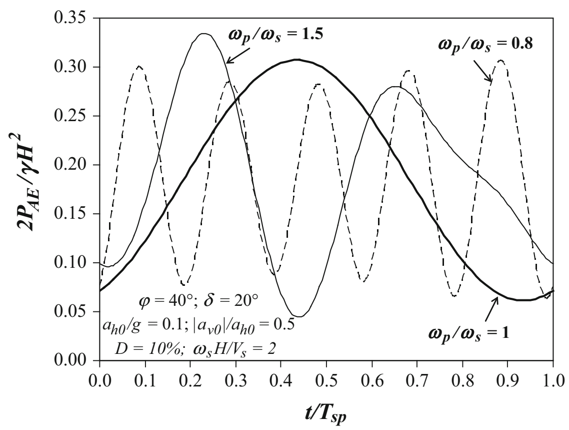

Fig. 13 Values of the normalized soil active thrust versus normalized time in the overall period T_{sp} for different values of ω_p/ω_s for $\varphi = 40°$; $\delta = 20°$; $a_{h0}/g = 0.1$; $|a_{v0}|/a_{h0} = 0.5$; $D = 10\ \%$; $\omega_s H/V_s = 2$

A value of ω_p/ω_s ($=T_s/T_p$) different from the unit implies that Q_h and Q_v have the same pair of values after a period T_{sp} generally greater than T_s and/or T_p. As an example for $\omega_p/\omega_s = 0.8$ $T_{sp} = 5T_s = 4T_p$ whereas for $\omega_p/\omega_s = 1.5$ $T_{sp} = 2T_s = 3T_p$, as shown in Fig. 12. Consequently, for $\omega_p/\omega_s \neq 1$ the seismic active thrust follows no longer a sinusoidal trend but a *cyclic* trend of period T_{sp} (Fig. 13).

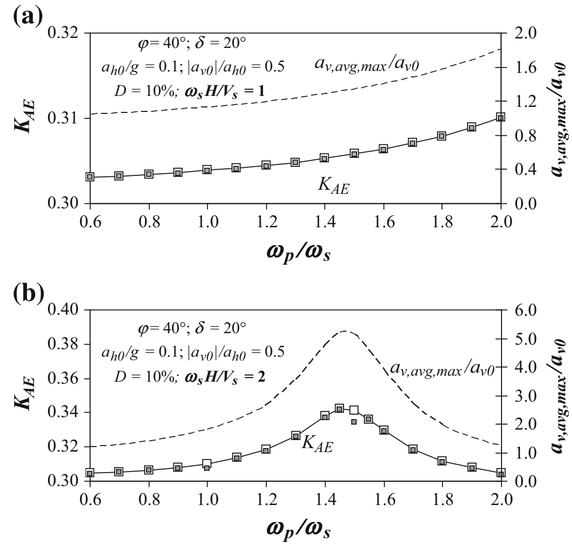

Fig. 14 Effect of frequency ratio ω_p/ω_s on seismic active soil coefficient for $\varphi = 40°$ $\delta = 20°$ $a_{h0}/g = 0.1$ $|a_{v0}|/a_{h0} = 0.5$; $D = 10\ \%$ (**a**) $\omega_s H/V_s = 1$; **b** $\omega_s H/V_s = 2$. *Solid symbols* refer to K_{AE} obtained by optimization procedure; *open symbols* and *line* refer to K_{AE} obtained assuming maxima inertia forces

Figure 14 shows the values of K_{AE} as a function of ω_p/ω_s for two different values $\omega_s H/V_s$, all other parameters being equal. In the same figure the open symbols represents the maximum values of K_{AE} obtained for $a_{h,avg} = a_{h,avg,max}$ and $a_{v,avg} = a_{v,avg,max}$ (i.e. assuming that horizontal and vertical inertia forces peak at the same instant). Generally the difference between the calculated K_{AE} and K_{AEmax} are found to be very small (<1 %). Greatest differences are found for $\omega_s H/V_s = 2$ and $\omega_p/\omega_s = 1$ and 1.5, i.e. at the lowest values of the overall period T_{sp} when it is more likely that Q_h and Q_v do not peak simultaneously.

Moreover it can be observed that in the investigated range of ω_p/ω_s (0.6–2) the trend of K_{AE} versus ω_p/ω_s depends on the value of the normalized frequency of S-wave; in particular for $\omega_s H/V_s = 1$ the trend is monotonically increasing (Fig. 14a), whereas for $\omega_s H/V_s = 2$ the trend shows a peak for $\omega_p/\omega_s = 1.45$ (Fig. 14b). This different trend is due to the different amplification of vertical acceleration within the soil wedge, plotted as dashed curve in Fig. 14. Indeed, in the hypothesis that $V_p = 1.87V_s$, for $\omega_s H/V_s = 1$ the normalized frequency of P-wave $\omega_p H/V_p$ ranges between 0.32 and 1.07, far from its fundamental frequency. On the contrary for $\omega_s H/$

Table 1 Comparison of seismic active earth coefficient (K_{AE}) obtained by the present study with those from the existing pseudo-dynamic method for $\omega_s H/V_s = 1$; $\omega_p = \omega_s$; $D = 10$ % $\varphi/\delta = 0.5$; $a_{v0} = 0.5a_{h0}$

a_{h0}/g	Existing pseudo-dynamic method with amplification[a]		Present study	
	$\varphi = 30°$	$\varphi = 40°$	$\varphi = 30°$	$\varphi = 40°$
0.05	0.357[b]	0.243	0.363	0.248
0.10	0.421	0.292	0.435	0.304
0.15	0.494	0.349	0.520	0.368
0.20	0.579	0.412	0.620	0.442
0.25	0.678	0.484	0.740	0.527

[a] Assuming the same amplification factors obtained by Eqs. (13)–(14); i.e. $f_{ah} = 1.782$, $f_{av} = 1.155$

[b] The value refers to the maximum K_{AE} obtained with $a_{v0} > 0$ and $a_{v0} < 0$

Table 2 Comparison of seismic active earth coefficient (K_{AE}) obtained by the present study with those from the existing pseudo-dynamic method for $\omega_s H/V_s = 2$; $\omega_p = \omega_s$; $D = 10$ % $\varphi/\delta = 0.5$; $|a_{v0}| = 0.5a_{h0}$

a_{h0}/g	Existing pseudo-dynamic method with amplification[a]		Present study	
	$\varphi = 30°$	$\varphi = 40°$	$\varphi = 30°$	$\varphi = 40°$
0.05	0.366[b]	0.250	0.366	0.250
0.10	0.441	0.308	0.440	0.307
0.15	0.529	0.375	0.526	0.372
0.20	0.633	0.452	0.626	0.447
0.25	0.824	0.547	0.805	0.534

[a] Assuming the same amplification factors obtained by Eqs. (13)–(14); i.e. $f_{ah} = 2.293$, $f_{av} = 1.980$

[b] The values refer to the maximum K_{AE} obtained with $a_{v0} > 0$ and $a_{v0} < 0$

$v_s = 2\ \omega_p H/v_p$ varies between 0.64 and 2.14, i.e. in a range containing the fundamental frequency of *P*-wave.

6.7 Comparison of Results

It has been previously noted that the new pseudo-dynamic method automatically includes amplification effects within the soil and that the average seismic accelerations through the soil wedge ($a_{h,avg}$ and $a_{v,avg}$) are generally greater than amplitude of accelerations at the base of the wall (a_{h0}, a_{v0}), as shown in Fig. 2. Consequently, it is obvious that the values of K_{AE} obtained by the present method can be much higher than those obtained with the pseudo-static approach using $k_h = a_{h0}/\text{g}$ and $k_v = a_{v0}/\text{g}$, especially close to the fundamental frequency of S-wave.

Similarly, the present method overestimates the values of K_{AE} in comparison with the values obtained using other pseudo-dynamic methods which neglect amplification effect. The recent procedure based on Rayleigh waves (Choudhury et al. 2014a, b) belongs to this category.

A meaningful comparison can be made only with the existing pseudo-dynamic method, provided that amplification factors are included in the analysis for both S-wave and P-wave, by assuming that amplitudes of seismic accelerations vary linearly from the base of the layer to the ground surface (Steedman and Zeng 1990; Choudhury and Nimbalkar 2007, 2008; Nimbalkar and Choudhury 2007; Kolathayar and Ghosh 2009). To make the seismic input uniform, two different amplification factors are considered for S-wave and P-wave (i.e. $f_{ah} \neq f_{av}$), according to Eqs. (13)–(14).

In Tables 1 and 2 a comparison of active earth pressure coefficients is presented for two different values of $\omega_s H/V_s$ varying the base horizontal acceleration ($a_{h0} = 0.05$–0.25 g) and soil shear resistance angle ($\varphi = 30$; $\varphi = 40°$), assuming the same damping ratio ($D = 10$ %) and the same frequency ($\omega_s = \omega_p$) for S-wave and P-wave.

Table 3 Comparison of seismic active earth coefficient (K_{AE}) obtained by the present study with those from some available theories for $\varphi/\delta = 0.5$; $k_v = a_{v0} = 0$; $\omega_s H/V_s = 1.885$; $\omega_p = \omega_s$; $D = 10$ %

k_h	Pseudostatic		Choudhury and Nimbalkar (2006)		Mylonakis et al. (2007)		Choudhury et al. (2014a)		Present study $\alpha_h = 1$ $a_{h0} = k_h/f_{ah}$		Present study $\alpha_h = 2/3$ $a_{h0} = 1.5k_h/f_{ah}$	
	$\varphi = 30°$	$\varphi = 40°$	$\varphi = 30°$	$\varphi = 40°$	$\varphi = 30°$	$\varphi = 40°$	$\varphi = 30°$	$\varphi = 40°$	$\varphi = 30°$	$\varphi = 40°$	$\varphi = 30°$	$\varphi = 40°$
0.0	0.305	0.201	0.305	0.201	0.305	0.201	0.30	0.20	0.305	0.201	0.305	0.201
0.1	0.368	0.253	0.361	0.247	0.368	0.253	0.37	0.27	0.349	0.238	0.377	0.260
0.2	0.452	0.319	0.434	0.305	0.458	0.324	0.48	0.35	0.407	0.283	0.476	0.337
0.3	0.563	0.402	0.528	0.376	0.588	0.425	0.58	0.44	0.475	0.337	0.611	0.436

Data shown in Table 1 indicate that for a normalized frequency $\omega_s H/V_s = 1$ the present method is more conservative than the existing pseudo-dynamic method. The differences between the values of K_{AE} increase at increasing base horizontal acceleration, from about 5 % for $a_{h0}/g = 0.15$ to about 9 % for $a_{h0}/g = 0.25$.

For a higher normalized frequency $\omega_s H/V_s = 2$ (Table 2) the present approach gives values of K_{AE} practically coincident with those of the existing pseudo-dynamic approach, with differences not exceeding 2 %.

It is well recognized that most of the available methods assume a constant acceleration in the soil using seismic coefficient k_h and k_v obtained from the maximum acceleration expected at the soil surface taking into account of stratigraphic amplification (see for example Eurocode 8):

$$k_h = \alpha_h a_{h,max}/g. \quad k_v = \pm\alpha_v k_h \tag{50}$$

where $\alpha_h \leq 1 \quad 1/3 \leq \alpha_v \leq 1/2$.

Therefore a more comprehensive comparison can be made assuming the same maximum acceleration instead of the same base acceleration. With this aim the seismic input must be adapted; in particular the present method requires to calculate the base acceleration considering amplification factors f_{ah} and f_{av} and Eq. (50), i.e. $a_{h0} = k_h g/(f_{ah}\alpha_h)$ and $a_{v0} = k_v g/(f_{av}\alpha_h)$.

Table 3 shows the numerical results for seismic active earth coefficient K_{AE} obtained from the present solution and some established solutions in the literature. For sake of simplicity the comparison is made neglecting the vertical acceleration for two different values of α_h ($\alpha_h = 1$ $\alpha_h = 2/3$). For the proposed and the existing pseudo-dynamic methods a normalized frequency of 1.885 (i.e. $H/V_s T_s = 0.3$) is assumed, according to previous studies on similar topic (Choudhury and Nimbalkar 2005, 2006; Ghosh 2007, 2010; Kolathayar and Ghosh 2009; Ghosh and Kolathayar 2011).

Results are in reasonable good agreement (largest discrepancy 16 %). As expected, the predictions given by the present method underestimate K_{AE} when $\alpha_h = 1$ because in other methods the acceleration is assumed to have its maximum amplitude through the entire wedge. On the contrary, the proposed approach leads to slightly conservative predictions of K_{AE} when the available approaches assume $\alpha_h = 2/3$ to calculate

k_h from the maximum acceleration. In this case the present approach can be more suitable for practical applications. Indeed it should be emphasized that the present method, unlike pseudo-static method and Mylonakis et al. analysis, allows to consider effect of time, as well as to predict a not linear pressure distribution along the back of the wall, according to experimental observations (e.g. Steedman and Zeng 1990).

7 Conclusions

The new pseudo-dynamic approach proposed by Bellezza (2014) has been extended taking into account both horizontal and vertical acceleration.

The proposed approach represents an improvement of the pioneering pseudo-dynamic approach for two main reasons: (1) standing seismic *S*-wave and *P*-wave respect the zero stress boundary condition at the ground surface and therefore both horizontal and vertical accelerations are naturally amplified within the backfill without the need of introducing an amplification factor; (2) a more realistic behavior of soil is accounted for by modeling the backfill as a visco-elastic medium.

Maintaining some hypotheses of the existing pseudo-dynamic method—including absence of water, homogeneous backfill and planar failure surface—inertia forces, seismic active thrust, active pressure distribution and overturning moment were derived in dimensionless form as a function of the normalized frequencies $\omega_s H/V_s$ and $\omega_p H/V_p$ and damping ratio D, assumed to be the same for both shear and primary wave.

The range of applicability of the pseudo-dynamic approach and the correlations with pseudo-static method have been also discussed by introducing the concept of weighted average acceleration.

The results of the parametric study substantially confirm the results previously obtained in the absence of the vertical acceleration; soil active thrust and pressure distribution are very sensitive to variation of amplitude of base horizontal acceleration, soil shear resistance angle and normalized frequency of shear wave, especially close to its fundamental frequency where the effect of damping is magnified. The effect of soil-wall friction angle is generally small.

Unlike the pioneering pseudo-dynamic approach, the effect of a different frequency for S- and P-wave has been investigated, highlighting that soil active thrust generally increases when P-wave have a frequency greater than that of S-wave.

The results obtained by the proposed method are found to be in agreement with previous studies, provided that the seismic input is adapted to include amplification effects.

References

Ahmad SM, Choudhury D (2008a) Pseudo-dynamic approach of seismic design for waterfront reinforced soil wall. Geotext Geomembr 26(4):291–301
Ahmad SM, Choudhury D (2008b) Stability of waterfront retaining wall subjected to pseudo-dynamic earthquake forces and tsunami. J Earthq Tsunami 2(2):107–131
Ahmad SM, Choudhury D (2009) Seismic design factor for sliding of waterfront retaining wall. Proc Inst Civ Eng Geotech Eng 162(5):269–276
ASTM D4015 (2007) Standard method for modulus and damping of soils by resonant-column method. ASTM International, West Conshohocken
Bellezza I (2014) A new pseudo-dynamic approach for seismic active soil thrust. Geotech Geol Eng 32(2):561–576
Bellezza I, D'Alberto D, Fentini R (2012) Pseudo-dynamic approach for active thrust of submerged soils. Proc Inst Civ Eng Geotech Eng 165(5):321–333
Choudhury D, Ahmad SM (2008) Stability of waterfront retaining wall subjected to pseudo-dynamic earthquake forces. J Waterw Port Coast Ocean Eng ASCE 134(4):252–262
Choudhury D, Katdare AD (2013) New approach to determine seismic passive resistance on retaining walls considering seismic waves. Int J Geomech ASCE 13(6):852–860
Choudhury D, Nimbalkar SS (2005) Seismic passive resistance by pseudo-dynamic method. Géotechnique 55(9):699–702
Choudhury D, Nimbalkar SS (2006) Pseudo-dynamic approach of seismic active earth pressure behind retaining wall. Geotech Geol Eng 24(5):1103–1113
Choudhury D, Nimbalkar SS (2007) Seismic rotational displacement of gravity walls by pseudo-dynamic method: passive case. Soil Dyn Earthq Eng 27(3):242–249
Choudhury D, Nimbalkar SS (2008) Seismic rotational displacement of gravity walls by pseudo-dynamic method. Int J Geomech ASCE 8(3):169–175
Choudhury D, Katdare AD, Pain A (2014a) New method to compute seismic active earth pressure on retaining wall considering seismic waves. Geotech Geol Eng 32(2):391–402
Choudhury D, Katdare AD, Shukla SK, Basha BM, Ghosh P (2014b) Seismic behaviour of retaining structures, design issues and requalification techniques. Indian Geotech J 44(2):167–182

Das BM (1993) Principles of soil dynamics. PWS–Kent Publishing Company, Boston

Eurocode 8 - EN 1998-5 (2005) Design of structures for earthquake resistance - Part 5: Foundations, retaining structures and geotechnical aspects. CEN European Committee for Standardization, Bruxelles

Fang YS, Chen TJ (1995) Modification of Mononobe–Okabe theory. Géotechnique 45(1):165–167

Ghosh P (2007) Seismic passive earth pressure behind non-vertical retaining wall using pseudo-dynamic analysis. Geotech Geol Eng 25(5):693–703

Ghosh P (2008) Seismic active earth pressure behind a non-vertical retaining wall using pseudo-dynamic approach. Can Geotech J 45(1):117–123

Ghosh S (2010) Pseudo-dynamic active force and pressure behind battered retaining wall supporting inclined backfill. Soil Dyn Earthq Eng 30(11):1226–1232

Ghosh P, Kolathayar S (2011) Seismic passive earth pressure behind non-vertical wall with composite failure mechanism: pseudo-dynamic approach. Geotech Geol Eng 29(5):363–373

Kolathayar S, Ghosh P (2009) Seismic active earth pressure on walls with bilinear backface using pseudo-dynamic approach. Comput Geotech 36(5):1229–1236

Kolsky H (1963) Stress waves in solids. Dover Publications, New York

Kramer SL (1996) Geotechnical earthquake engineering. Pearson Education, New Jersey 1996

Mononobe N, Matsuo H (1929) On the determination of earth pressures during earthquakes. Proc World Eng Congr, Tokyo, pp 177–185

Mylonakis G, Klokinas P, Papantonopoulus C (2007) An alternative to the Mononobe-Okabe equations for seismic earth pressure. Soil Dyn Earthq Eng 27(10):957–969

Nimbalkar SS, Choudhury D (2007) Sliding stability and seismic design of retaining wall by pseudo-dynamic method for passive case. Soil Dyn Earthq Eng 27(6):497–505

Nimbalkar SS, Choudhury D, Mandal JN (2006) Seismic stability of reinforced-soil wall by pseudo-dynamic method. Geosynth Int 13(3):111–119

Okabe S (1926) General theory of earth pressures. J Jpn Soc Civ Eng JSCE 12(1):123–134

Steedman RS, Zeng X (1990) The influence of phase on the calculation of pseudo-static earth pressure on retaining wall. Géotechnique 40(1):103–112

Yuan C, Peng S, Zhang Z, Liu Z (2006) Seismic wave propagation in Kelvin–Voigt homogeneous visco-elastic media. Sci China, Ser D Earth Sci 49(2):147–153